https://doi.org/10.1016/j.compstruct.2019.111378
This is the Pre-Published Version.

(Title Page)

Effects of surface contact on the dynamic responses of delaminated composite plates

Yi He[1], Yi Xiao[1*], Zhongqing Su[2]

(1. School of Aerospace Engineering and Applied Mechanics Tongji University, Shanghai 200092, China)

(2. Department of Mechanical Engineering the Hong Kong Polytechnic University, Hong Kong, China)

Corresponding author: +86 2165983674. Email: y_xiao@tongji.edu.cn

Abstract: This paper investigates the modal parameters such as the damping ratio, frequency and shape of delaminated composite plates with contact properties. The contact damping is analyzed using a viscoelastic Coulomb friction model with sliding phase, which combines energy dissipation of sliding friction and sticky friction. Finite element method (FEM) based models simulate the dynamic responses of delaminated composite plates, in which the constant normal contact stiffness and contact damping are introduced via penalty stiffness method and equivalent viscous damping, respectively. Relevant vibration experiments are set up to obtain the modal parameters of delaminated composite plates. The results show that the modal damping ratio of the composite laminated plates increases significantly with increase in the delamination percentage, and the contact damping plays a major role in the increase of the modal damping ratio. Furthermore, the contact stiffness also has a minor influence on the modal frequency and shape of delaminated composite plates. The experimental data is consistent with simulations, thereby establishing the accuracy of the FEM model.

Keywords: laminated composites; delamination; contact damping; penalty stiffness; finite element method

© 2019. This manuscript version is made available under the CC-BY-NC-ND 4.0 license http://creativecommons.org/licenses/by-nc-nd/4.0/.

(Text)

1 Introduction

A new generation of highly advanced composite materials are gradually replacing traditional metals for structural applications. However, throughout their service life period, composite material parts are subject to extreme work conditions such as impact, high-stress-amplitude periodic load and high interface stress. As a result, various defects are inevitably generated. One of the main failure modes is delamination, which causes a dramatic reduction in the structural capability for compression and shear resistance. Since, these factors pose a serious threat to the structural safety, early detection and diagnosis of delamination in composite material structures is necessary to achieve long term operation.

The most mature and practical assessment method detects changes in the dynamic parameters. Zou et al. [1] observed that showed that the structural dynamic response varied significantly when delamination damage occurred in composite laminates, which was mainly reflected in the change of modal parameters. Modal parameter analysis is an important approach for delamination identification, mainly consisting of three components: modal shape, modal frequency and modal damping. Early studies focused on building analytical dynamic models to accurately calculate the modal frequencies of delaminated composite plates. Experimental and theoretical results [2-5] showed that the change of frequencies of delaminated composite plates in early and middle stages (delamination percentage ≤50%) has less practical usage on the early diagnosis for delamination. Subsequently, Ju [6], Shen [7] and Luo [8] surveyed the modal shape analysis and observed no significant difference between the shape of the delaminated plates and the intact plates in the first 6-ordermodes. To circumvent the demerits of modal frequencies and modal shape, more recent works have diverted their attention to modal damping. Modal damping can provide relatively higher sensitivity in the early stage of delamination, which is very suitable to serve as a detection parameter.

Calculations of the first several orders of modal damping performed by Saravanos [3], Luo [4] and Yim [9] led to a constant forecast modal damping, which was inconsistent with experiments and showed a significant increasing trend. A plausible explanation is that only the material damping was considered in those works and they only considered the type of modal damping related on the change of modal shape. Since these studies removed adverse interference (e.g. boundary conditions and air damping), there could be an internal energy dissipation mechanism in the delaminated structure, which is generally considered to be interfacial friction. Generally, dry friction model is the primary option for calculating internal friction behavior in delamination. Studies relating to dry friction model such as investigations by Wang [10], Cameron [11], Bazan [12] and Menq [13] considered that the energy dissipation only occurs in the sliding phase, and does not exist in the sticky phase (or pre-sliding phase). Evidently, this hypothesis is not applicable for calculating interaction between two viscoelastic media like resin matrix of composite material, since there would be part of energy consumed

by viscosity of interfacial material. To overcome this limitation, Polycarpou [14], Olsson [15], Andersson [16] and Al-Bender [17] took the viscosity into account in the sticky phase, establishing a viscous Coulomb friction model. However, they ignored the contact stiffness that existed in sticky phase of original Coulomb friction.

Furthermore, another aspect that needs improvement in order to obtain precise dynamic simulation of delaminated composite material is modeling the contact interaction using the finite element method (FEM). Luo and Hanagud [8] used spring connections to set constraints on the upper and lower contact surfaces of the delamination. Their results showed that the spring stiffness had a minor effect on the structural frequency response, and the calculated values were generally higher than the experimental values. It indicates that the FEM modeling method may impart unrealistic and excessive structural stiffness due to the unreleased constraint in the opening phase. In order to release this superfluous constraint, Ju [18], Żak [19] and Singh [20] used the penalty stiffness method for calculating the frequency response of the delaminated composite plates. Results indicated that this method could accurately reflect the property of delaminated contact. However, these studies did not provide guidelines for choosing the appropriate penalty stiffness. As an important branch of vibration-based NDT methods, the Poincaré map method also receives increasing attention, owning to its sensitivity of detecting system's nonlinearity. Manoach [21] took advantage of Poincaré map to analysis the response of damaged laminated beams, modeled by geometrically nonlinear version of Timoshenko beam theory, under large vibration load and temperature change. The result showed that a significant phase diagram divergence occurred, in spite of narrow natural frequencies between damaged/nondamaged beams. An improved version of Poincaré map method was developed [22], by which an excellent result obtained indicated its potential application in on-line SHM because of its efficiency using lower-dimensional state space. This paper aims to establish a theoretical model describing the contact damping mechanism of delaminated composite plates undergoing dynamic movements. A 3D FEM modeling method with specific definitions of contact damping and contact stiffness is developed using the ABAQUS software package to precisely simulate contact interaction of delamination in dynamic condition. Based on the established models, 1st-order modal damping ratios of delaminated composite plates are calculated; various dynamic responses are simulated by the built FEM method, which are compared with experimental results for verification. Finally, the effect of contact stiffness on stimulated dynamic response results is discussed.

2 Modal damping of delaminated composite plates

2.1 Material damping

In order to obtain the damping of the overall structure, the material damping should be first taken into account. The specific damping capacity model (SDC) and complex modulus approach have been extensively used for prediction of damping at micromechanical, macromechanical and structural levels in laminated composites [23-25]. So far, the complex modulus approach subroutine can only be implemented in linear perturbation steps, which is

ineffective for simulating the model containing contact interaction. Therefore, in this paper, SDC is adopted. The main principle of SDC is that the total specific damping capacity ψ of the structure can be characterized by the quotient obtained by dividing energy dissipation ΔU by total conservative energy U in one cycle:

$$\psi = \frac{\Delta U}{U} \tag{1}$$

In FEM, ΔU and U can be calculated by summing the dissipated energy of every element and strain energy. Eq. (1) can then be expressed as:

$$\psi_{\text{material}} = \frac{\Delta U_{\text{material}}}{U} = \frac{\sum_{k=1}^{N} \int_{V_k^e} \frac{1}{2} \boldsymbol{\sigma}_k^{e\mathrm{T}} \boldsymbol{\Psi} \boldsymbol{\varepsilon}_k^e \mathrm{d}V_k^e}{\sum_{k=1}^{N} \int_{V_k^e} \frac{1}{2} \boldsymbol{\sigma}_k^{e\mathrm{T}} \boldsymbol{\varepsilon}_k^e \mathrm{d}V_k^e} \tag{2}$$

Where, ψ_{material} is the material specific damping capacity.

2.2 Contact damping

Contact damping is generated when two interfaces possess mechanical interaction. When there is tangential relative motion, friction is typically the major energy dissipation mechanism.

Table 1 summarizes three current mainstream dry friction models: 1) classical Coulomb friction model, 2) elastic Coulomb friction model (with tangential contact stiffness in sticky stage) and 3) viscous Coulomb friction model (with tangential viscosity coefficient in sticky stage). Coulomb friction model and its modified forms reflect the relationship between the frictional force and tangential deformation in the sticky stage. Both sliding friction and static friction exist when there is weak contact, which is the case for delamination. In such conditions, normal and tangential contact stiffness act at the contact interface, so the models in Table 1 need to be combined. Therefore, a viscoelastic Coulomb friction model is established in this section (see Fig.1).

In the sticky phase, Kelvin viscoelasticity can be used to describe the relationship between static friction equivalent tangential contact modulus G_{contact}, static friction equivalent tangential viscous damping coefficient c_{contact}, interface tangential stress τ_{contact} and strain γ_{contact} caused by static friction:

$$\tau_{\text{contact}} = G_{\text{contact}} \gamma_{\text{contact}} + c_{\text{contact}} \dot{\gamma}_{\text{contact}} \tag{3}$$

In general, due to the surface roughness, G_{contact} and c_{contact} may be slightly different compared to interfacial material modulus and viscosity coefficient. Here, the effect of roughness is omitted for the sake of simplicity. Hence, it is acceptable to treat G_{contact} and c_{contact} as shear modulus and viscosity coefficient of resin matrix, or $G_{\text{contact}} = 891.30\text{MPa}$, $c_{\text{contact}} = G_{\text{contact}} \left(2\xi_{\text{matrix}} / \omega_r\right)$ ($\xi_{\text{matrix}} \approx 0.8\%$). In r^{th} order modes, micro slip in stick stage s_{c} of a certain contact pair is expressed as follows:

$$s_{\text{c}} = s_{\text{a}} \sin\left(\omega_r t\right) \tag{4}$$

Then, γ_{contact} is given by:

$$\gamma_{\text{contact}} = \frac{s_{\text{c}}}{h} = \frac{s_{\text{a}} \sin(\omega_r t)}{h} \tag{5}$$

Substituting Eq. (4) into Eq. (5):

$$\tau_{\text{contact}} = \frac{G_{\text{contact}} s_{\text{c}}}{h} \pm \frac{c_{\text{contact}} \omega_r \sqrt{s_{\text{a}}^2 - s_{\text{c}}^{\ 2}}}{h} \tag{6}$$

Where, $h = 0.005\text{mm}$ [26]. Eq. (6) can be transformed into quadratic form:

$$\frac{\left(h\tau_{\text{contact}} - G_{\text{contact}} s_{\text{c}}\right)^2}{c_{\text{contact}}^{\ 2} \omega_r^2 s_{\text{a}}^2} + \frac{s_{\text{c}}^{\ 2}}{s_{\text{a}}^2} = 1 \tag{7}$$

Intuitively, this quadratic curve is a slanted elliptical hysteresis loop, which has been presented by red solid line in Fig. 2. The surrounded area represents the energy dissipation of this contact pair in a cycle:

$$\Delta U_{\text{contact_p}} = \frac{c_{\text{contact}} \omega_r s_a^2 \pi}{h} \tag{8}$$

Eq. (8) does not contain sliding phase. When F_{T} exceeds the maximum static frictional force (assumed same as sliding frictional force), the hysteresis loop cannot maintain a complete ellipse and tends to flatten at the top and bottom. The point of maximum stress in the hysteresis loop is the beginning of flat top, the corresponding s_{c} is:

$$\pm \frac{s_{\text{a}} G_{\text{contact}}}{\sqrt{G_{\text{contact}}^2 + c_{\text{contact}}^2 \omega_r^2}} \tag{9}$$

It is worth noting that $c_{\text{contact}} \omega_r \gg G_{\text{contact}}$, so Eq. (9) is approximately equal to s_{a}, which indicates that the point of maximum stress does not coincide with the point of maximum micro slip. This has been exaggerated in Fig. 2 for visualization purpose. In a realistic situation, these two points are extremely close. Hence, they are defaulted to coincide for simplification of calculation. After the flattening effect is produced, the original hysteresis loop generates a parallelogram region, and the new hysteresis loop becomes:

$$\tau_{\text{contact}} = \begin{cases} \dfrac{G_{\text{contact}}\left(s + s_{\text{b}}\right)}{h} + \dfrac{c_{\text{contact}} \omega_r \sqrt{s_{\text{a}}^{\ 2} - \left(s + s_{\text{b}}\right)^2}}{h}, & \dot{s} \geq 0 \wedge s \leq \left(s_{\text{a}} - s_{\text{b}}\right); \\ \dfrac{G_{\text{contact}} s_{\text{a}}}{h}, & \dot{s} \geq 0 \wedge s > \left(s_{\text{a}} - s_{\text{b}}\right); \\ \dfrac{G_{\text{contact}}\left(s - s_{\text{b}}\right)}{h} - \dfrac{c_{\text{contact}} \omega_r \sqrt{s_{\text{a}}^{\ 2} - \left(s - s_{\text{b}}\right)^2}}{h}, & \dot{s} < 0 \wedge s \geq \left(s_{\text{b}} - s_{\text{a}}\right); \\ \dfrac{G_{\text{contact}} s_{\text{a}}}{h}, & \dot{s} < 0 \wedge s < \left(s_{\text{a}} - s_{\text{b}}\right); \end{cases} \tag{10}$$

The new expanded hysteresis loop is shown by black solid line in Fig. 2. After appending the energy dissipation, the new $\Delta U_{\text{contact_p}}$ becomes:

$$\Delta U_{\text{contact_p}} = \frac{c_{\text{contact}}\omega_r s_{\text{a}}^2 \pi}{h} + 4\frac{G_{\text{contact}}}{h}\left(s_{\text{a}} + s_{\text{b}}\right) \tag{11}$$

Integrating Eq. (11) over the contact domain (i.e. delamination) yields the total contact energy dissipation:

$$\Delta U_{\text{contact}} = \int_A \Delta U_{\text{contact_p}} \mathrm{d}A = \int_A \left[\frac{c_{\text{contact}}\omega_r s_{\text{a}}^2 \pi}{h} + 4\frac{G_{\text{contact}}}{h}\left(s_{\text{a}} + s_{\text{b}}\right)\right]\mathrm{d}A \tag{12}$$

Referring to SDC, the contact specific damping capacity can also be written as follows:

$$\psi_{\text{contact}} = \frac{\Delta U_{\text{contact}}}{U} \tag{13}$$

Then, the total specific damping capacity is given as follows:

$$\psi = \psi_{\text{material}} + \psi_{\text{contact}} \tag{14}$$

Using the damping ratio form to represent ψ :

$$\xi = \frac{\psi}{4\pi} \tag{15}$$

3 FEM modeling for delaminated composite plates

3.1 Contact simulation

The complexity and difficulty of contact arises from its strong nonlinearity and discontinuity. In order to overcome this difficulty, 3D implicit FEM modeling of contact issue is processed in ABAQUS software, in which there is stable advanced control for contact problem. A comprehensive method is used to introduce the contact in the 3D FEM model of delaminated composite plate. This not only simulates the real contact boundary conditions, but also provides good convergence performance to output sufficiently accurate results as fast as possible. Therefore, a surface-to-surface-discretization constraint formation scheme is selected because of its higher accuracy than node-to-surface-discretization, which avoids serious enormous penetration of master surface into slave surface.

To set contact properties, hard contact is defined to formulate the pressure-overclosure relationship in normal direction. Doing this can minimize the penetration of the slave surface into the master surface, which will cost less time than softened contact in implicit algorithm computationally. The relationship between pressure p and overclosure h_{over} is given in software documentation as (Fig. 3):

$$\begin{cases} p = 0,\ h_{\text{over}} \le 0; \\ p > 0,\ h_{\text{over}} > 0; \end{cases} \tag{16}$$

The penalty method has been chosen to enforce constraints in this work. It involves a linear or nonlinear relationship between p and h_{over}, which represents a realistic physical meaning in contact issue: the relationship between p and normal deformation of contact layer (Fig. 4). The linear penalty method is presented by the following equation:

$$p = Kh_{\text{over}} \tag{17}$$

K has units of MPa/mm, which is different from the static friction equivalent contact modulus. The detailed relationship between penalty stiffness and contact modulus will be discussed in section 3.2.

3.2 Penalty stiffness

In previous reports, only a software generated default penalty stiffness has been considered that influences the convergence mathematically. However, once it is given a physical meaning, a precise value needs to be arrived at. Turning contact modulus into penalty stiffness is in fact a dimensional transformation. This transaction can be started from the constitutive relation in finite element:

$$\boldsymbol{\sigma}^e = \boldsymbol{QBa}^e \tag{18}$$

Where, $\boldsymbol{QB}$ can be replaced by $\boldsymbol{S}$:

$$\boldsymbol{S} = \boldsymbol{QB} \tag{19}$$

Then, $\boldsymbol{S}$ can be expended as follows:

$$\boldsymbol{S} = \left[\boldsymbol{QB}_1 \quad \cdots \quad \boldsymbol{QB}_8\right] = \left[\boldsymbol{S}_1 \quad \cdots \quad \boldsymbol{S}_8\right] \tag{20}$$

Where, $\boldsymbol{B}_n$ and $\boldsymbol{S}_n$ represent the nth submatrix of $\boldsymbol{B}$ and $\boldsymbol{S}$, respectively. Each submatrix of $\boldsymbol{S}$ contains the component in normal direction:

$$\boldsymbol{S}_{n,33} = \frac{E_{\text{contact}}\left(1-v_{\text{contact}}\right)\left(\xi_0 \pm \xi\right)\left(\eta_0 \pm \eta\right)}{8\xi_0\eta_0\zeta_0\left(1+v_{\text{contact}}\right)\left(1-2v_{\text{contact}}\right)},\ \left(n=1,\cdots,8\right) \tag{21}$$

$\boldsymbol{S}_{n,33}$ is a constant as it does not include any independent variable alone normal direction. Assuming that the deformation of element in normal direction is Δh, the normal stress can be obtained by the following equation:

$$\sigma_{33} = \sum_{k=1}^{8} S_k a_{33,k} = \frac{E_{\text{contact}}\left(1-v_{\text{contact}}\right)}{2\zeta_0\left(1+v_{\text{contact}}\right)\left(1-2v_{\text{contact}}\right)}\Delta h \tag{22}$$

An intuitive constitutive relationship between normal stress and normal deformation has been extracted out, and it can be assigned to K:

$$K = \frac{E_{\text{contact}}\left(1-v_{\text{contact}}\right)}{2\zeta_0\left(1+v_{\text{contact}}\right)\left(1-2v_{\text{contact}}\right)} \tag{23}$$

3.3 Introduction of tangential properties

For tangential property in FEM, the contact damping coefficient needs to be introduced. The normal contact damping coefficient ϑ_n in FEM software is defined as follows:

$$\vartheta_n = \frac{f_{e,n}}{A_e v_{e,n}} \tag{24}$$

The unit of this coefficient is $\mathrm{MPa \cdot s/mm}$. FEM software only has the direct access to the normal damping coefficient. If a tangential contact damping coefficient ϑ_t is required to be prominent, a large tangent fraction needs to be defined. Tangent fraction is the proportion of ϑ_t to ϑ_n, which is typically set to 0 by default. In this paper, its value is taken to be 1000 in order to highlight the effect of tangential damping. Actually, selection of tangent fraction is a user-based decision, balancing the calculation efficiency and accuracy. Result of trial calculation feedbacks an expected excessive-damping error when using a less value, due to superabundance of normal damping. On the other hand, though setting a larger value seems to be more realistic, the stability and convergence of calculation decrease, aborted in a worst situation.

3.4 Damping calculation and dynamic analysis process based on FEM

In order to obtain material damping and contact damping of delaminated composite plates, it is necessary to know stress, strain, volume of integration point, contact pressure and sliding distance. For a linear system such as intact plate, damping can be readily solved and introduced in models by *Frequency* step and *Modal dynamics* step (Italic characters represent software jargons in ABAQUS). However, this approach cannot be employed in the contact problem. Therefore, *Dynamic, Implicit* step is employed, which can effectively simulate the dynamic response of the delaminated composite plates with contact setup. A detailed flowchart concerning the procedure is presented in Fig. 5.

4 Dynamic experiment

4.1 Specimens and experimental method

Test material is carbon fiber/epoxy (T300/7901) prepreg supplied by Weihai Guangwei Composite Materials Co., Ltd., China. The triple symmetric orthogonal layup $[0/90_2/0_2/90_2/0]_s$ is selected, which can ensure non-tension-shear coupling in upper and lower sub-plates of the delaminated plates. The layups of delaminated composite plates are $[0/90_2/0//0/90_2/0]_s$ and $[0/90_2/0_2/90_2/0//]_s$ for offset and central delaminated plates, respectively, where "//" represents delamination. A Teflon film acts as the debonding layer laminated in the interlayers to form offset/central delamination. The length of delamination is a constant at 40 mm. For comparing the influence of different extents of delamination, 5 delaminated composite plates are chosen with the following lengths: 90 mm (corresponding to 44.4% delamination percentage), 130 mm (30.8%), 170 mm (23.5%), 210 mm (19.0%) and 250 mm (16.0%). Specimen geometry is

shown in Fig. 6.

Free decay method is used to measure 1st-modal damping ratio, as shown in the schematic in Fig. 6. Testing procedure involves the following: 1) exciting the structure by pulse, 2) measuring the free decay curve of the structure in the first-order mode and 3) fitting the extremums in the curve to obtain the damping ratio.

The fitting function is given as follow:

$$x = A\exp\left(-\xi\,\omega_{\mathrm{d}}t\Big/\sqrt{1-\xi^2}\right)\sin\left(\omega_{\mathrm{d}}t+\theta\right) \tag{25}$$

There is a monotonically increasing relationship between ξ and 1st-modal frequency [29]:

$$\xi = c\ln\left(\frac{\omega_{\mathrm{d}}}{2\pi}\right)+d \tag{26}$$

Where, c and d are two unknown parameters that are identified by fitting experimental data.

4.2 Determination of basic parameters

When calculating the material modal damping of delaminated composite plates using SDC, it is necessary to obtain the shear specific damping components (ξ_{11} , ξ_{22} , ξ_{12}) along the 0° , 90° principal directions and in-plane direction by performing free decay experiment on the 0°, 90° and 45° unidirectional laminates, respectively (Fig. 7). Damping data at different frequencies is obtained by measuring plates with different total lengths. Both the mechanical parameters and specific damping components are listed in Table 2.

To verify the accuracy of specific damping components, the 1st-modal damping ratio of intact laminated composite plates is calculated as described in Section 4.1 and the results are compared with experimental values (Fig. 8). Overall, the analytical result is consistent with the experimental results. Some significant errors between 60−80 Hz are attributed to coincident resonance frequency of the holder.

5 Results and discussion

5.1 Contact damping and free decay time-domain response

Combining the contact information regarding contact stresses and contact relative displacements, the 1st-order modal contact damping ratio is calculated using the raised viscoelastic Coulomb friction model, as shown in Fig. 9. An increasing trend of the modal damping ratio can be observed with increasing delamination percentage in both the offset and central delaminated plates. This trend grows more significantly in central plates than offset counterparts. In addition, the theoretical results of pure contact damping ratio (dashed line in Fig. 9) is also presented. When comparing the data of the intact plates, the contact damping effect can be considered to be the dominant factor for the increase in the modal damping ratio. Most theoretical results exhibit a relatively precise match with experimental values compared to previous reports, with the exception of the 44.4% central delamination case, which may be due to the unstable experimental result due to higher error.

In order to visually reflect the influence of contact damping on the energy absorption capacity of delaminated plates, the free decay time-domain responses of 30.8% and 44.4% delamination plates and their corresponding intact plates are simulated by attaching the damping properties in the nondamped FEM model. Fig. 10(a) and Fig. 10(b) show the results of offset and central delaminated plates, respectively. Experimental and FEM results of the four specimens indicate that a higher decay rate is observed for larger delamination percentages. For the same delamination percentage, central delamination results in a faster decay rate than the offset case.

5.2 Frequency-domain response

To discuss the effect of delamination on structural stiffness, experimental and FEM frequency-domain results corresponding to Fig. 10 are shown in Fig. 11. In these frequency-domain responses, the modal frequency is observed to shift with different delamination. The following shifts are observed: 0.51 Hz (Exp.)/0.50 Hz (FEM) for 30.8% offset, 14.8 Hz (Exp.)/16.02 Hz (FEM) for 44.4% offset, 1.27 Hz (Exp.)/3.00 Hz (FEM) for 30.8% central and 16.85 Hz (Exp.)/20.02 Hz (FEM) for 44.4% central.

From these results, it is evident that modal frequencies of all four samples decrease with the increasing of delamination percentage, with the central delamination causing larger frequency shifting.

Since the modal frequencies are related to the overall structural stiffness, the shifting phenomenon embodies the effect of delamination on structural stiffness reduction. A lager delamination can cause more obvious reduction in the structural stiffness, with the central delamination exhibiting a significant structural stiffness reduction.

5.3 Vibration shapes

Under low frequency conditions, since the wavelength is larger than the geometry of delamination region, the transmission directly crosses the delamination. Hence, only the overall response is analyzed. For studying the local effect of delamination, a comparison is carried out between the high-frequency simulations of intact plate and 44.4% delaminated plate. Table 3 shows the results of vibration shapes at three instances when a 100 kHz single sine wave is transmitted into each specimen. The wave is transmitted from the right side (free side) to the left side (fixed side). The scale remains the original setting on x/y axis, and is magnified 50 times in z axis for obvious display.

When the wave propagates in intact plate, there is no waveform change, and the amplitude is only decayed due to the influence of the material damping. However, when the same wave propagates in the 44.4% delaminated plate, it is significantly distorted, especially on the thin side. This result indicates that high frequency excitation is able to generate the wave containing information about the location of delamination, because the wavelength of high frequency excitation is shorter than the size of delamination, the high frequency wave cannot cross over delamination as easily as the low frequency wave.

5.4 Parameter discussion

There are two contact parameters influencing the dynamic responses of delaminated composite plates: contact stiffness and the contact damping. The contact damping is related to the precise modal shape, which further depends on correct structure stiffness. Hence, the effect of contact stiffness on dynamic response of the delaminated plate needs to be explored in depth.

Several simulations are performed on the 44.4% delaminated plate where the effect of three contact stiffness levels, 100% K, 10% K and 1% K on the frequency spectrum is studied, as shown in Fig. 12. As the contact stiffness level is decreased, the frequency-shifting occurs. A shift of 0.13 Hz is observed when 100% K to 10% K and 0.96 Hz when 10% K to 1% K. From this result, we observe that a smaller contact stiffness would cause lower modal frequency, since it weakens the overall structure stiffness. But overall, there is just slight changing in low frequency domain. The modal frequency shifting rates are 0.05% and 0.38% for 10% K and 1% K, respectively.

From the results in section 5.3, in high frequency domain, the locality of delamination appears, which could also be affected by contact stiffness. Therefore, the time domain responses of the three nodes with 100%K, 10%K and 1%K are simulated under identical excitations as section 5.3. The location of three nodes has been pointed out in Fig. 13. Sampling nodes 1 and 3 are located on non-delaminated (Ndl) area 1 and 2, respectively. The sampling node 2 is located on delaminated (Dl) area.

Two significant results are summarized here. Firstly, compared with the data of the intact plate, the time-domain responses of delaminated plate are similar in Ndl areas 1 and 2, whereas a strong amplitude leap is observed in the Dl Area. This again reflects the locality of delamination under high frequency excitation. Secondly, the effect of contact stiffness also has locality in this situation. Although, the three curves in Fig. 13 basically coincide on Ndl area 1 and 2, a large change happens on Dl area. The curves of 100% K and 10% K are still narrow, but 1% K one is magnified.

6 Conclusions

This paper discusses the effects of surface contact on the dynamic responses of delaminated composite plates. A new friction model combining the Kelvin viscoelasticity energy dissipation in sticky phase and sliding energy dissipation is developed to calculate the contact damping in delaminated composite plates. A novel 3D delaminated composite plates FEM modeling method with specific contact stiffness and contact damping coefficient is also established. Conclusions based on the experiments and FEM predictions of the modal parameters of delaminated composite plates are summarized as follows:

(1) Contact occurring between delamination interfaces during vibration produces energy dissipation. The main source of energy dissipation is the internal friction containing both viscoelastic sticky phase and sliding phase.

(2) The penalty method can effectively simulate the contact between delamination

interfaces that are generally challenging to observe in experiments. Additionally, the penalty stiffness value has a specific relationship with the actual contact layer modulus in the FEM.

(3) Experiments and theoretical results are consistent for 1st-order modal damping ratio analysis. An increasing trend of 1st-order modal damping ratio with the delamination percentage is observed in both offset and central delaminated composite plates. Moreover, central delamination leads to a larger increase in the 1st-order modal damping ratio.

(4) Small frequency shifts are observed in delaminated composites plates with increasing delamination percentage, with the central delamination exhibiting greater shifts. This phenomenon also indicates that delamination causes a reduction in the structural stiffness.

(5) The locality of delamination can appear by high frequency excitation. If its wavelength is shorter than delamination size, the wave is distorted when it passes through delamination area. In time-domain responses, the strong amplitude leap appears in delaminated area.

(6) The contact stiffness has a slight effect in low frequency spectrum, where a smaller contact stiffness leads to a larger frequency decrease. A significant influence in delaminated area appears under high frequency excitation.

Acknowledgements

This research was funded by the National Natural Science Foundation of China (Grant No.11832014) and Hitachi Construction Machinery Co. Ltd. (Japan) as a part of a project on HSSF-High strength steel fatigue characteristics (1330-239-0009).

Reference

[1] Zou Y, Tong L, Steven G P. Vibration-based model-dependent damage (delamination) identification and health monitoring for composite structures—a review. Journal of Sound and vibration, 2000, 230(2): 357-378.

[2] Pardoen G C. Effect of delamination on the natural frequencies of composite laminates. Journal of composite materials, 1989, 23(12): 1200-1215.

[3] Saravanos D A, Hopkins D A. Effects of delaminations on the damped dynamic characteristics of composite laminates: analysis and experiments. Journal of Sound and Vibration, 1996, 192(5): 977-993.

[4] Luo H, Hanagud S. Delamination detection using dynamic characteristics of composite plates//36th Structures, Structural Dynamics and Materials Conference. 1995: 1172.

[5] Żak A, Krawczuk M, Ostachowicz W. Numerical and experimental investigation of free vibration of multilayer delaminated composite beams and plates. Computational Mechanics, 2000, 26(3): 309-315.

[6] Ju F, Lee H P, Lee K H. Finite element analysis of free vibration of delaminated composite plates. Composites engineering, 1995, 5(2): 195-209.

[7] Shen M H H, Grady J E. Free vibrations of delaminated beams. Aiaa Journal, 1992, 30(5):1361-1370.

[8] Luo H, Hanagud S. Dynamics of delaminated beams. International Journal of Solids & Structures, 2000, 37(10):1501-1519.

[9] Yim J H, Jang B Z. Damping in partially delaminated composites. Ksme International Journal, 1997, 11(5):537-546.

[10] Wang J H, Chen W K. Investigation of the vibration of a blade with friction damper by HBM//ASME 1992 International Gas Turbine and Aeroengine Congress and Exposition. American Society of Mechanical Engineers, 1992: V005T14A003-V005T14A003.

[11] Cameron T M, Griffin J H. An alternating frequency/time domain method for calculating the steady-state response of nonlinear dynamic systems. Journal of applied mechanics, 1989, 56(1): 149-154.

[12] Bazan E, Bielak J, Griffin J H. An efficient method for predicting the vibratory response of linear structures with friction interfaces. Journal of engineering for gas turbines and power, 1986, 108(4): 633-640.

[13] Menq C H, Griffin J H, Bielak J. The influence of a variable normal load on the forced vibration of a frictionally damped structure. Journal of Engineering for Gas Turbines and Power, 1986, 108(2): 300-305.

[14] Polycarpou A A, Soom A. Application of a two-dimensional model of continuous sliding friction to stick-slip. Wear, 1995, 181: 32-41.

[15] Olsson H, Åström K J, De Wit C C, et al. Friction models and friction compensation. Eur. J. Control, 1998, 4(3): 176-195.

[16] Andersson S, Söderberg A, Björklund S. Friction models for sliding dry, boundary and mixed lubricated contacts. Tribology international, 2007, 40(4): 580-587.

[17] Al-Bender F, Lampaert V, Swevers J. The generalized Maxwell-slip model: a novel model for friction simulation and compensation. IEEE Transactions on automatic control, 2005, 50(11): 1883-1887.

[18] Ju F, Lee H P, Lee K H. Dynamic response of delaminated composite beams with intermittent contact in delaminated segments. Composites Engineering, 1994, 4(12): 1211-1224.

[19] Żak A, Krawczuk M, Ostachowicz W. Vibration of a laminated composite plate with closing delamination. Journal of Intelligent Material Systems and Structures, 2001, 12(8): 545-551.

[20] Singh A K, Chen B Y, Tan V B C, et al. Finite element modeling of nonlinear acoustics/ultrasonics for the detection of closed delaminations in composites. Ultrasonics, 2017, 74: 89-98.

[21] Manoach E, Samborski S, Mitura A, et al. Vibration based damage detection in composite beams under temperature variations using Poincaré maps. International Journal of Mechanical Sciences, 2012, 62(1): 120-132.

[22] Manoach E, Warminski J, Kloda L, et al. Numerical and experimental studies on vibration based methods for detection of damage in composite beams. Composite Structures, 2017, 170: 26-39.

[23] Lin D X, Ni R G, Adams R D. Prediction and measurement of the vibrational damping parameters of carbon and glass fibre-reinforced plastics plates. Journal of composite materials, 1984, 18(2): 132-152.

[24] Berthelot J-M, Assarar M, Sefrani Y, El-Mahi A. Damping analysis of composite materials and structures. Composite Structures, 2008, 85(3):189–204.

[25] He Y, Xiao Y, Liu Y, et al. An efficient finite element method for computing modal damping of laminated composites: Theory and experiment. Composite Structures, 2018, 184: 728-741.

[26] Zhang Zhen. Study on Vibration Loosening Characteristics and Detection of Fastener Connections. Shanghai: Tongji University, 2017. (In Chinese)

[27] Hu B G, Dokainish M A. Damped vibrations of laminated composite plates—modeling and finite element analysis. Finite elements in analysis and design, 1993, 15(2): 103-124.

[28] Tian H, Li B, Liu H, et al. A new method of virtual material hypothesis-based dynamic modeling on fixed joint interface in machine tools. International Journal of Machine Tools and Manufacture, 2011, 51(3): 239-249.

[29] Adams R D, Bacon D G C. Measurement of the flexural damping capacity and dynamic Young's modulus of metals and reinforced plastics. Journal of Physics D: Applied Physics, 1973, 6(1): 27.

Nomenclature

ψ	Total specific damping capacity
ΔU	Energy dissipation in a cycle
U	Total conservative energy in a cycle
ψ_{material}	Material specific damping capacity
$\Delta U_{\text{material}}$	Material energy dissipation
$\boldsymbol{\sigma}_k^e$	Stress vector of the kth element
$\boldsymbol{\Psi}$	Material damping capacity matrix
$\boldsymbol{\varepsilon}_k^e$	Strain vector and volume of the kth element
V_k^e	Volume of the kth element
N	Total amount of elements
F_{N}	Normal load
F_{T}	Tangential load
f_{T}	Frictional force
μ	Friction coefficient
s_{c}	Micro slip in stick stage
$k_{\text{N-C}}$	Normal contact stiffness
$k_{\text{T-C}}$	Tangential contact stiffness
c_{contact}	Static friction equivalent tangential viscous damping coefficient
G_{contact}	Static friction equivalent tangential contact modulus
τ_{contact}	Interfacial tangential stress caused by static friction
γ_{contact}	Interfacial tangential strain caused by static friction
ξ_{matrix}	Damping ratio of matrix material
ω_r	r^{th} order modal frequency
s_{a}	Maximum micro-slip deformation in the static friction

h	Thickness of deforming contact layer
$\Delta U_{\text{contact_p}}$	Energy dissipation of a contact pair in a cycle
s_{b}	Half of macro slip deformation in sliding phase
$\Delta U_{\text{contact}}$	Total contact energy dissipation
A	Delaminated area
ψ_{contact}	Contact specific damping capacity
ξ	Damping ratio
p	Pressure
h_{over}	Overclosure
K	Penalty stiffness
$\boldsymbol{\sigma}^{e}$	Stress vector of element
$\boldsymbol{a}^{e}$	Displacement vector of element
$\boldsymbol{Q}$	Constitutive matrix
$\boldsymbol{B}$	Strain matrix of element
$\boldsymbol{S}$	Stress matrix of element
E_{contact}	Elastic modulus of contact material
ν_{contact}	Poisson's ratio of contact material
ϑ_{n}	Normal contact damping coefficient in FEM software
$f_{\text{e,n}}$	Normal damping force of contact mode
A_{e}	Node area
$v_{\text{e,n}}$	Relative normal speed of contact node
ϑ_{t}	Tangential contact damping coefficient
A	Vibration amplitude
ω_{d}	Circular frequency of damped structure

Table and Figure Captions:

Fig. 1. Mechanism of modified Kelvin viscoelastic static friction with sliding phase.

Fig. 2. Hysteresis loops (▬: Kelvin viscoelastic static friction; ▬: modified Kelvin viscoelastic static friction with sliding phase)

Fig. 3. Pressure-overclosure relationship in penalty method.

Fig. 4. Equivalent node overclosure quoted from deformation of contact layer.

Fig. 5. Solving procedure combined with FEM.

Fig. 6. Schematic diagram of (a) specimen geometry and (b) experimental setup of the procedure.

Fig. 7. Experimentally measured 1st-order frequency-dependent damping ratio for unidirectional laminates. (▬: Fitting, ■: Exp.; Color pictures in e-edition, same thereinafter)

Fig. 8. Measured and fitted 1st-order frequency-dependent damping ratio for cross-ply laminated plates.

Fig. 9. Experiment (Exp.) and theoretical (The.) results of 1st-order damping ratio for delaminated composite plates: (a) Offset delaminated samples, (b) Central delaminated samples.

Fig. 10. Calculated and measured free decay time-domain responses of delaminated composite plates: (a) Offset delaminated samples, (b) Central delaminated samples (▬: Del.; ▬: Intact)

Fig. 11 Calculated and measured frequency-domain responses of delaminated composite plates (Calculated by Steady-state dynamics, Direct): (a) Offset delaminated samples, (b) Central delaminated samples.

Fig. 12. Calculated frequency-domain responses of 44.4% delaminated composite plates with different K .

Fig. 13. Calculated time-domain responses of 44.4% offset delaminated plate and corresponding intact plate excited by one-cycle 100 kHz sine wave.

Table 1 Properties of different dry friction models.

Table 2 Material properties of T300/7901 Carbon/Epoxy composite material used in FEM simulation.

Table 3 Calculated vibration shapes of 44.4% offset delaminated plate and corresponding intact plate excited by one-cycle 100kHz sine wave.

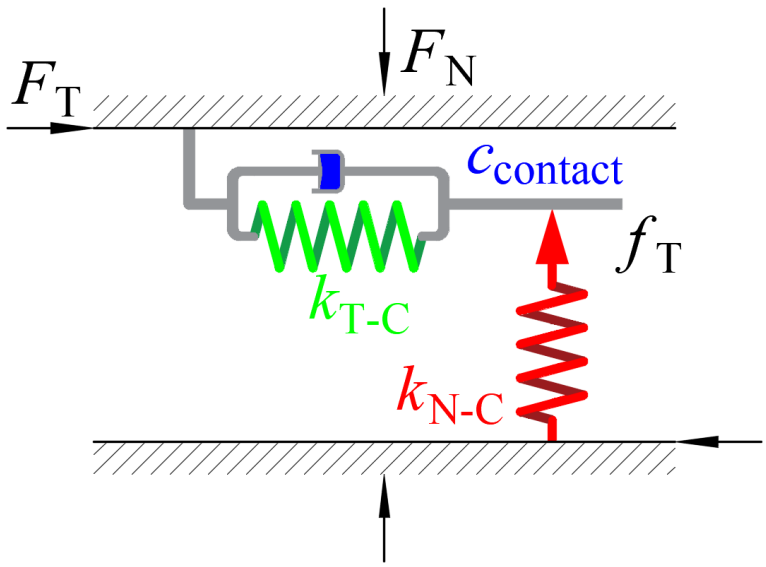

Fig. 1. Mechanism of modified Kelvin viscoelastic static friction with sliding phase.

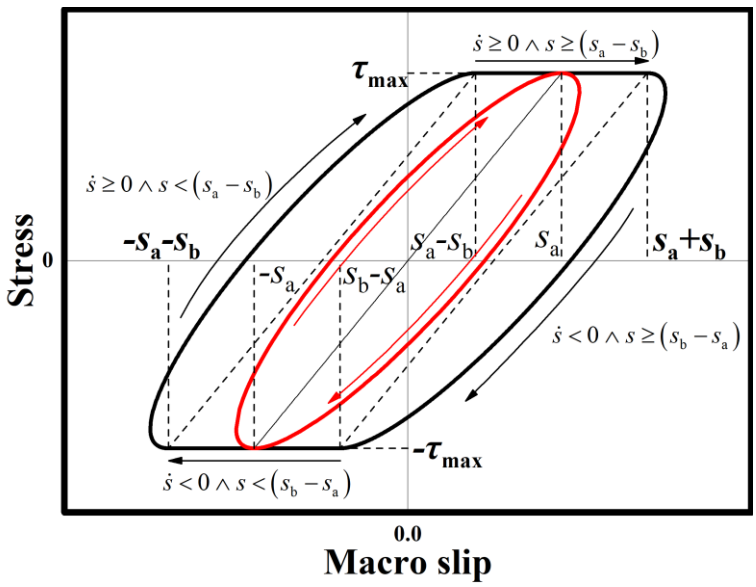

Fig. 2. Hysteresis loops (▬: Kelvin viscoelastic static friction; ▬: modified Kelvin viscoelastic static friction with sliding phase)

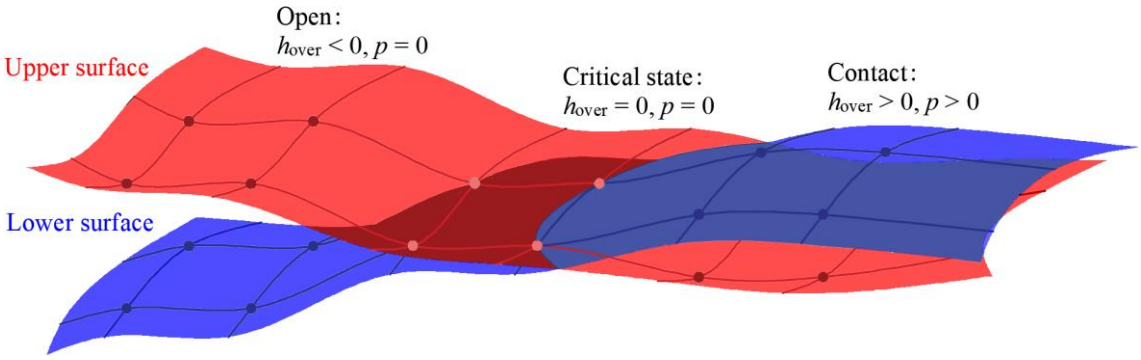

Fig. 3. Pressure-overclosure relationship in penalty method.

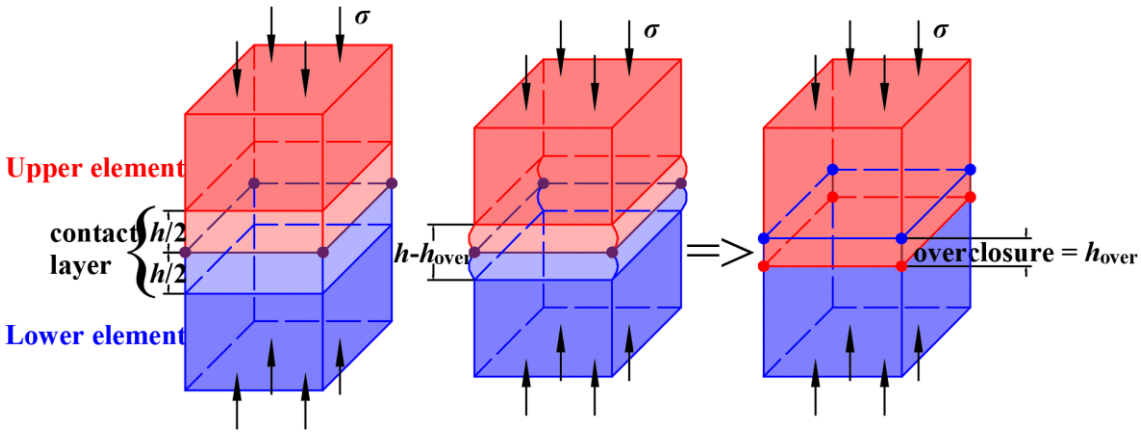

Fig. 4. Equivalent node overclosure quoted from deformation of contact layer.

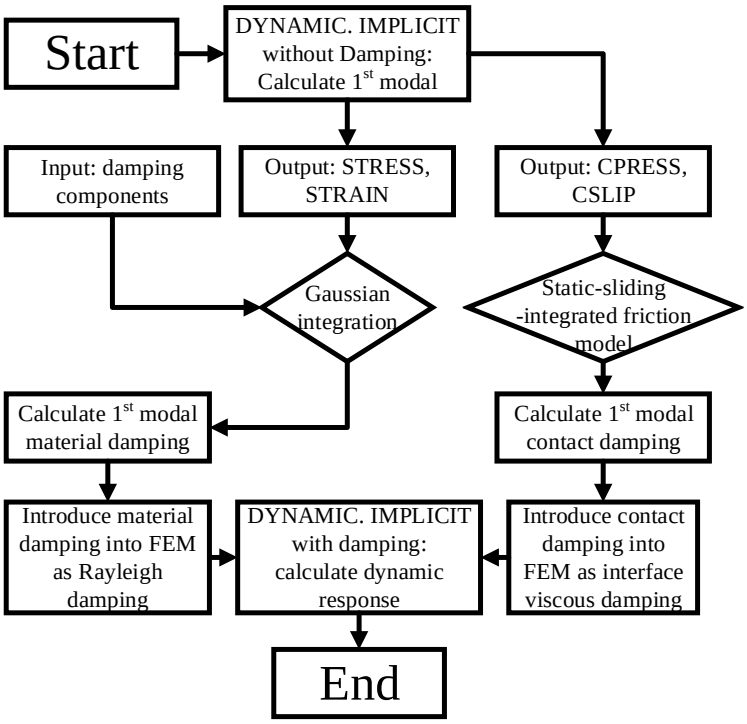

Fig. 5. Solving procedure combined with FEM.

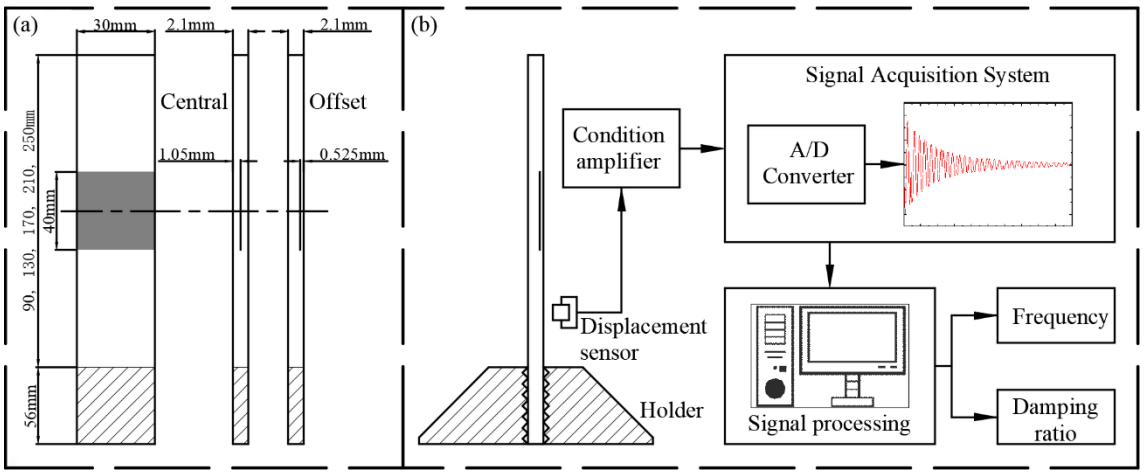

Fig. 6. Schematic diagram of (a) specimen geometry and (b) experimental setup of the procedure.

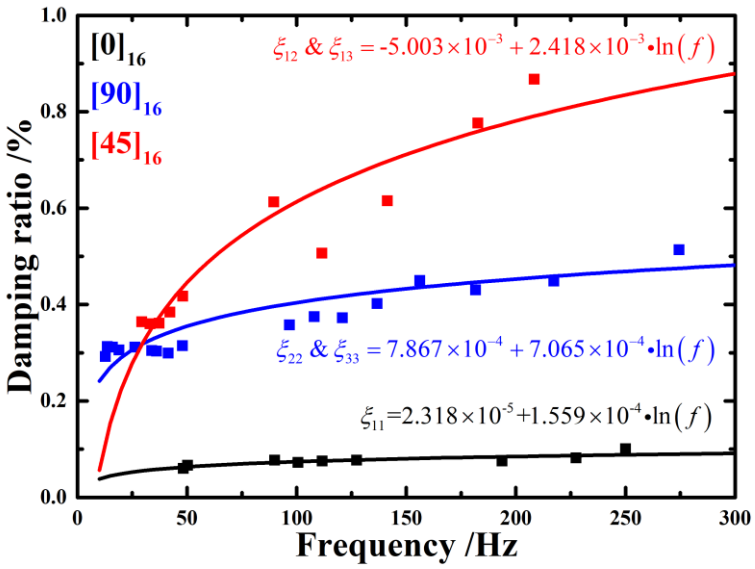

Fig. 7. Experimentally measured 1st-order frequency-dependent damping ratio for unidirectional laminates. (▬:Fitting, ■: Exp.; Color pictures in e-edition, same thereinafter)

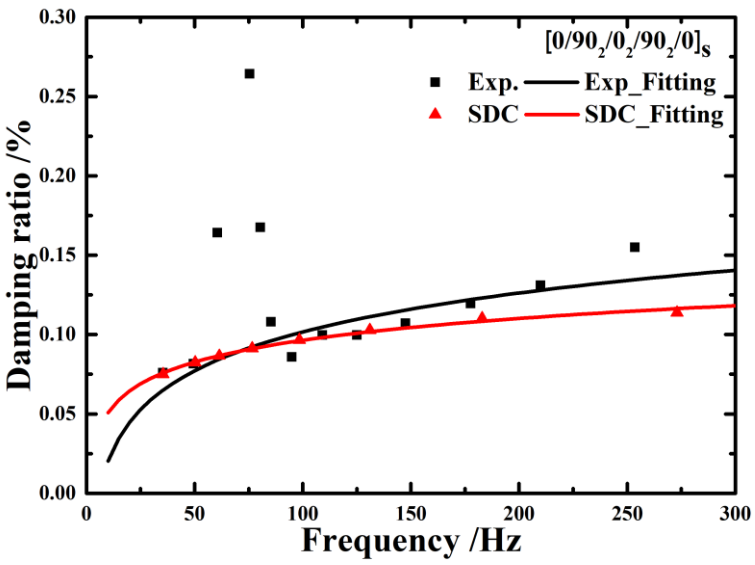

Fig. 8. Measured and fitted 1st-order frequency-dependent damping ratio for cross-ply laminated plates.

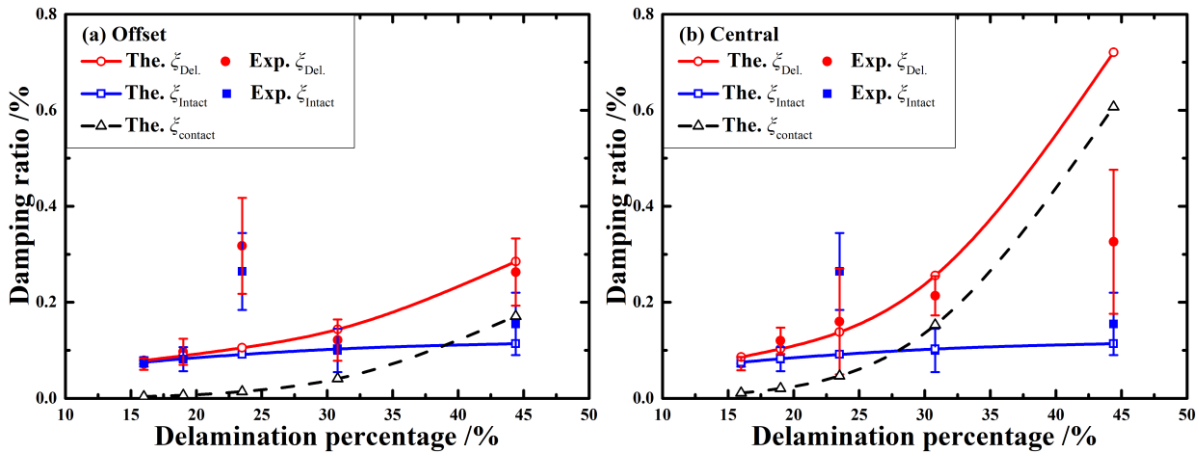

Fig. 9. Experiment (Exp.) and theoretical (The.) results of 1st-order damping ratio for delaminated composite plates: (a) Offset delaminated samples, (b) Central delaminated samples.

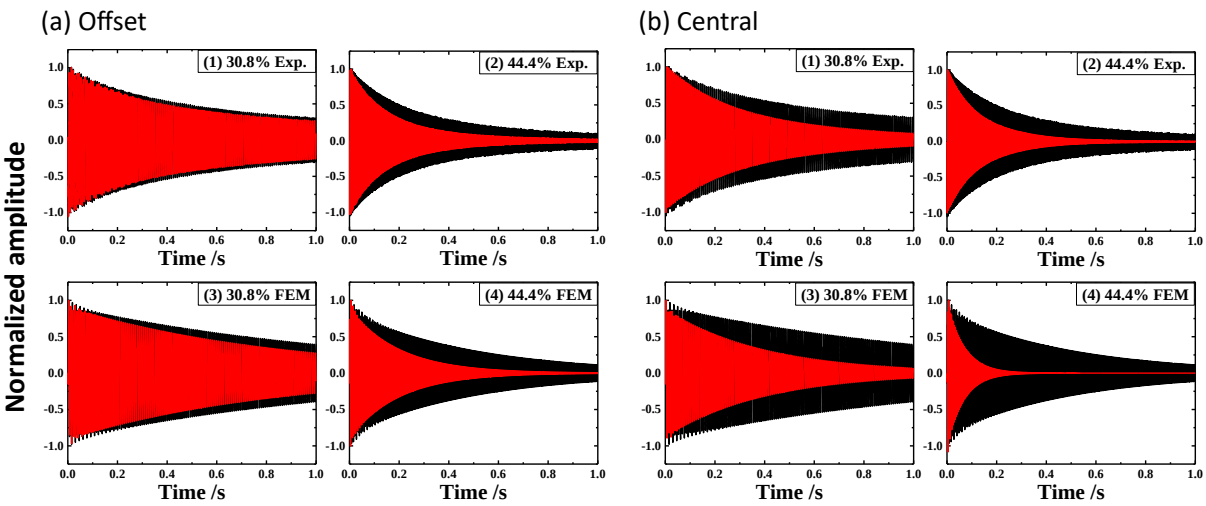

Fig. 10. Calculated and measured free decay time-domain responses of delaminated composite plates: (a) Offset delaminated samples, (b) Central delaminated samples (▬: Del.; ▬: Intact)

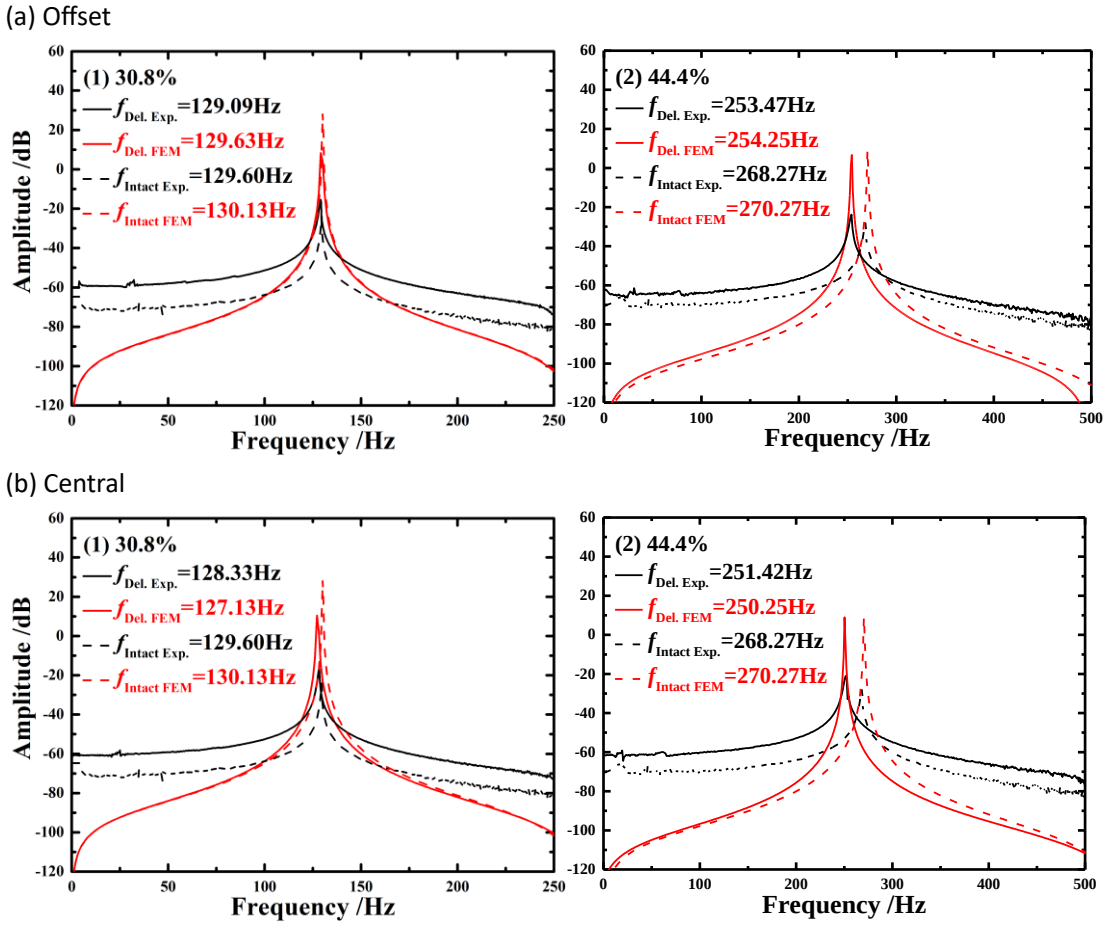

Fig. 11 Calculated and measured frequency-domain responses of delaminated composite plates (Calculated by Steady-state dynamics, Direct): (a) Offset delaminated samples, (b) Central delaminated samples.

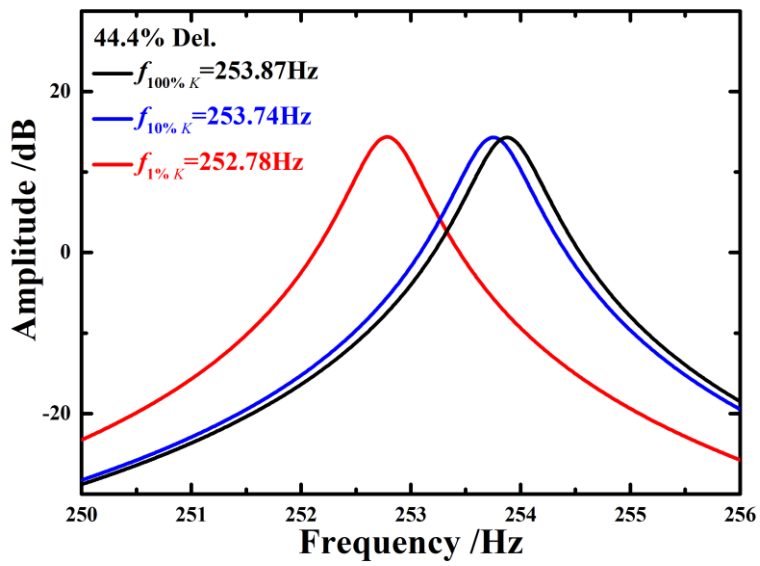

Fig. 12. Calculated frequency-domain responses of 44.4% delaminated composite plates with different K .

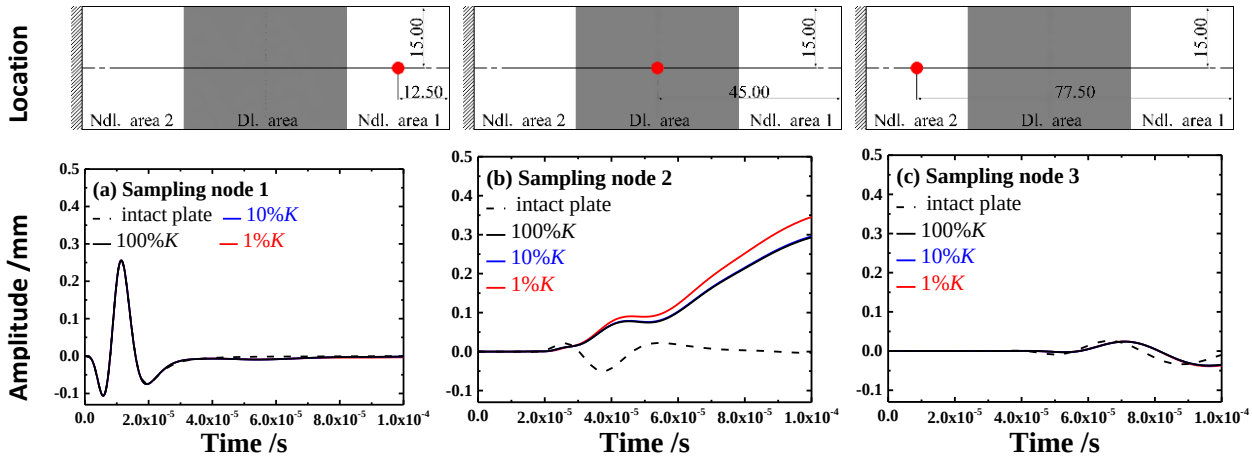

Fig. 13. Calculated time-domain responses of 44.4% offset delaminated plate and corresponding intact plate excited by one-cycle 100 kHz sine wave.

Table 1 Properties of different dry friction models.

Dry friction model	Mechanism	F_T - s relationship	Hysteresis loop
Classical Coulomb friction model [12]	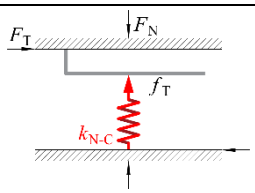	$f_T = \begin{cases} \mu F_N, F_T \geq \mu F_N; \\ F_T, s_c = 0, F_T < \mu F_N; \end{cases}$	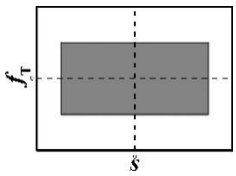
Elastic Coulomb friction model [10, 11, 13]	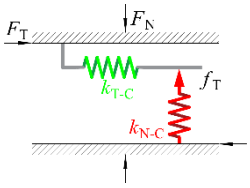	$f_T = \begin{cases} \mu F_N, F_T \geq \mu F_N; \\ k_{T\text{-}C} s_c = F_T, F_T < \mu F_N; \end{cases}$	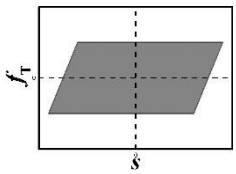
Viscous Coulomb friction model [16]	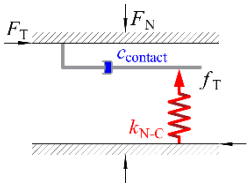	$f_T = \begin{cases} \mu F_N, \lvert c_{contact} \dot{s}_c \rvert \geq \mu F_N; \\ c_{contact} \dot{s}_c, \lvert c_{contact} \dot{s}_c \rvert < \mu F_N; \end{cases}$	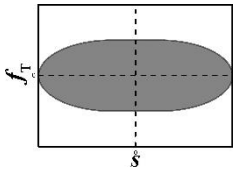

Table 2 Material properties of T300/7901 Carbon/Epoxy composite material used in FEM simulation.

Mechanical parameters		Specific damping components	
E_{11} (GPa)	130.0	ξ_{11}	$2.318\times10^{-5}+1.559\times10^{-4}\ln\left(f_{1^{st}\text{-order}}\right)$
E_{22} & E_{33} (GPa)	7.64	ξ_{22} & ξ_{33}	$7.867\times10^{-4}+7.065\times10^{-4}\ln\left(f_{1^{st}\text{-order}}\right)$
G_{12} & G_{13} (GPa)	3.7	ξ_{12} & ξ_{13}	$-5.003\times10^{-3}+2.418\times10^{-3}\ln\left(f_{1^{st}\text{-order}}\right)$
G_{23} (GPa)	3.0	ξ_{23}	$\frac{\xi_{12}}{2}$
ν_{12} & ν_{13}	0.32	$\xi_{\nu12}$ & $\xi_{\nu13}$	0
ν_{23}	0.45	$\xi_{\nu23}$	0
ρ (kg/m^3)	1690	——	——

Table 3 Calculated vibration shapes of 44.4% offset delaminated plate and corresponding intact plate excited by one-cycle 100kHz sine wave.

Time /s	Intact plate	Offset delaminated plate
2×10^{-5}	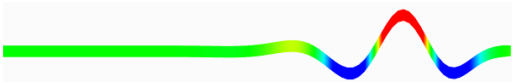	
4×10^{-5}	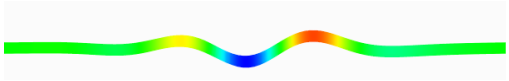	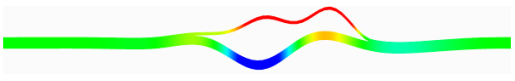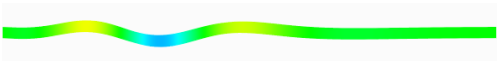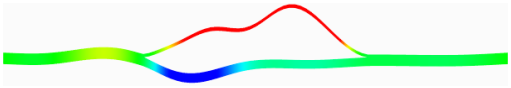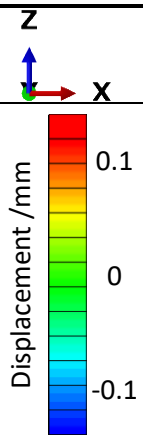
6×10^{-5}